Supporting Information

Polydopamine encapsulation of fluorescent nanodiamonds for biomedical applications

*Hak-Sung Jung, Kyung-Jin Cho, Yeonee Seol, Yasuharu Takagi, Andrew Dittmore, Paul A. Roche, and Keir C. Neuman**

Table S1. Reaction conditions determine shell thickness of PDA encapsulated FNDs. Reactions were performed in 10mM TRIS buffer, pH=8.5 with 0.2 mg FND (80 nm, 1 mg/mL) in a total volume of 10 ml for a final FND density of 0.02 mg/mL. The reaction time and dopamine concentration were varied, and the resulting shell thickness was measured from TEM images as described in the main text and methods. The shell thickness is the mean of ten measurements and the Standard Deviation is reported as the uncertainty in the measurement.

Sample	Dopamine (mM)	Time (hr)	Thickness (nm)
1	0.59	2	2.7 ± 0.8
2	0.73	2	3.0 ± 1.0
3	0.92	2	6.9 ± 2.4
4	1.14	2	9.1 ± 1.6
5	1.42	0.5	2.9 ± 0.5
6	1.42	1	5.2 ± 1.2
7	1.42	1.5	11.3 ± 1.3
8	1.42	2	15.4 ± 3.5

Table S2. Average PL intensity of individual FND and FND@PDA of different sizes measured by TIRFM. The PL intensity measured for *N* particles in three different fields of view on the slide is reported as the mean ± S.D. The relative intensity of the encapsulated FNDs is reported as a percentage of the bare FND PL. The FNDs were encapsulated with PDA for 1 hr at 1.42 mM DA concentration (line 6 in table S1).

Sample	Average PL intensity	Sample	Average PL intensity
20 nm FND	**0.031 ± 0.001 (100%)** N=608	**20 nm FND@PDA**	**0.025 ± 0.005 (81.5%)** N=281
40 nm FND	**0.032 ± 0.004 (100%)** N=662	**40 nm FND@PDA**	**0.024 ± 0.003 (75.3%)** N=420
80 nm FND	**1.757 ± 0.173 (100%)** N=47	**80 nm FND@PDA**	**0.919 ± 0.156 (52.3%)** N=68
150 nm FND	**0.174 ± 0.029 (100%)** N=50	**150 nm FND@PDA**	**0.131 ± 0.019 (75.2%)** N=53

Table S3. Average PL intensity of individual FND (80 nm) and FND@PDA measured by TIRF. The "thick shell" sample corresponds to Sample 8 conditions that result in an average shell thickness of 15.4 ± 3.5 nm (line 8 in table S1), whereas the "thin shell" samples correspond to Sample 5 conditions that yield an average shell thickness of 2.9 ± 0.5 nm (Line 5 in Table S1).

	FND Intensity (AU)	**FND@PDA (thick shell) Intensity (AU)**	**FND@PDA (thin shell) Intensity (AU)**
Average	**0.14 ± 0.01 (100%)** N=393	**0.05 ± 0.00 (35%)** N=305	**0.09 ± 0.01 (64%)** N=123

Table S4. Zeta-potential of FND, PDA, FND@PDA, and PEGylated FND@PDA. All particles were dispersed in deionized water. The solution including particles were injected into a folded capillary cell (DTS1060). After the cell was placed into the Zetasizer and equilibrated at 25 °C, measurements were performed for 3 times. The reported error corresponds to the standard deviation.

Sample	**Potential (mV)**
FND	–32.6 ± 0.4
PDA	–43.5 ± 0.3
FND@PDA	–43.6 ± 1.0
FND@PDA-PEG	–39.7 ± 0.5

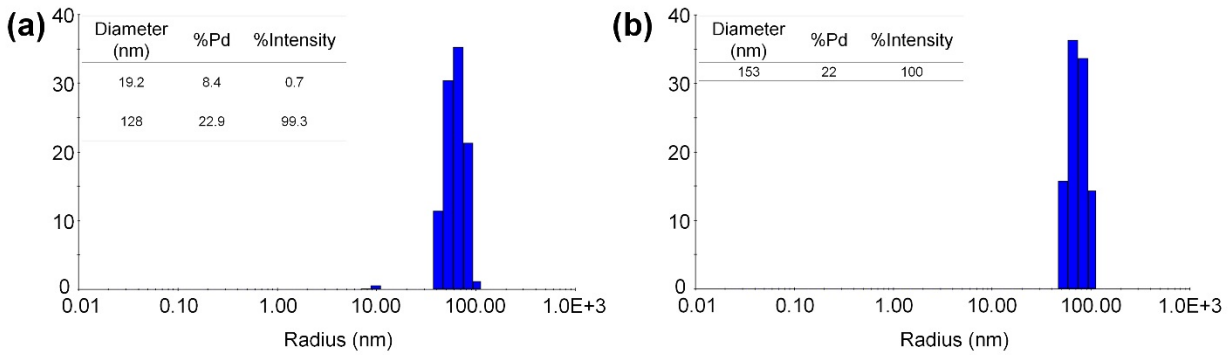

Figure S1. DLS based measurements of hydrodynamic diameter of (a) bare 80 nm FND and (b) PDA-coated FND (2 hr reaction for PDA coating with 1.42 mM DA concentration – line 8 in Table S1) in water. The curves represent the distribution of mass weighted particle sizes and the reported diameters correspond the mean of each peak. DLS measurements and analysis are described in the Methods section of the main text.

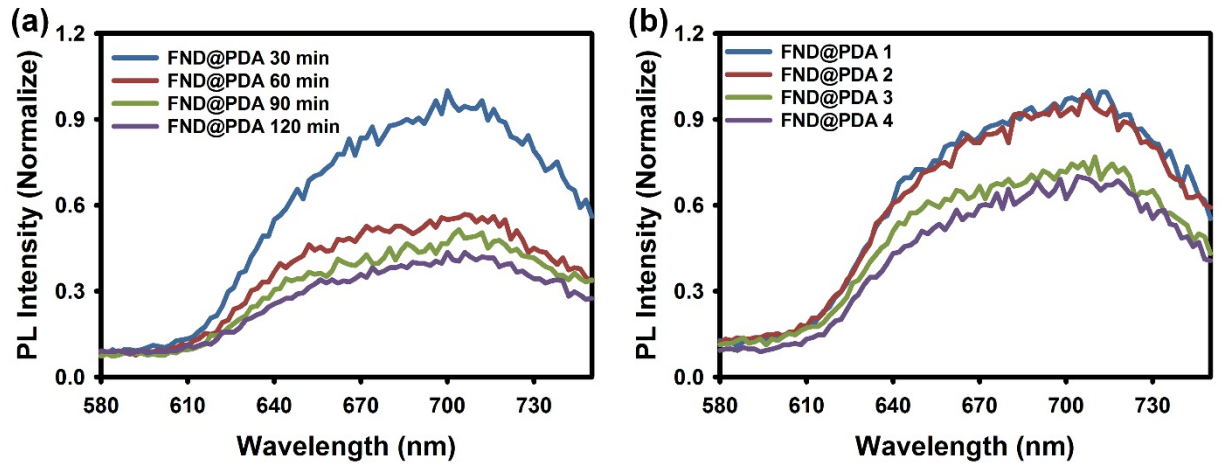

Figure S2. Normalized PL spectra of PDA-coated FND as function of reaction time (a) and dopamine concentration (b). 80 nm FND was encapsulated with different reaction conditions (Table 1). Each spectrum was normalized by maximum PL intensity of each reaction conditions such as 30 min PDA coating (line 5 in Table S1) or minimum concentration of dopamine (line 1 in Table S1).

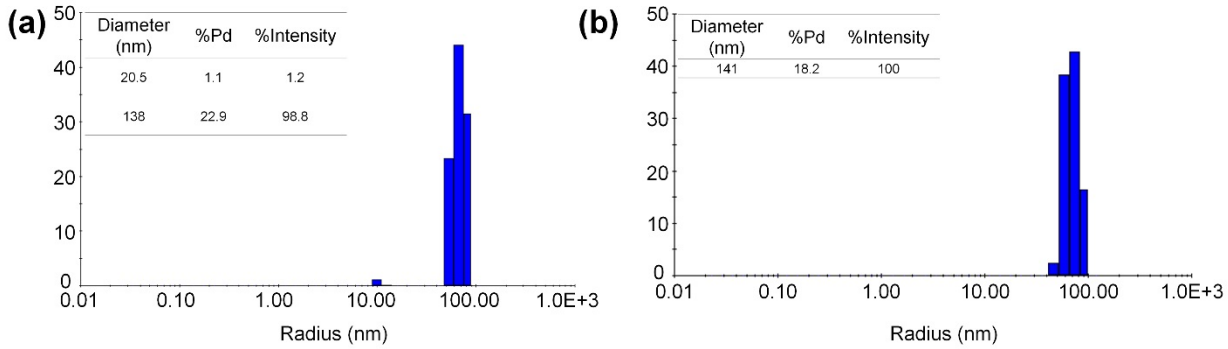

Figure S3. DLS based measurements of hydrodynamic diameter of (a) FND@PDA (30 min reaction for PDA coating with 1.42 mM DA concentration – line 5 in Table S1) and (b) FND@PDA-PEG in water.

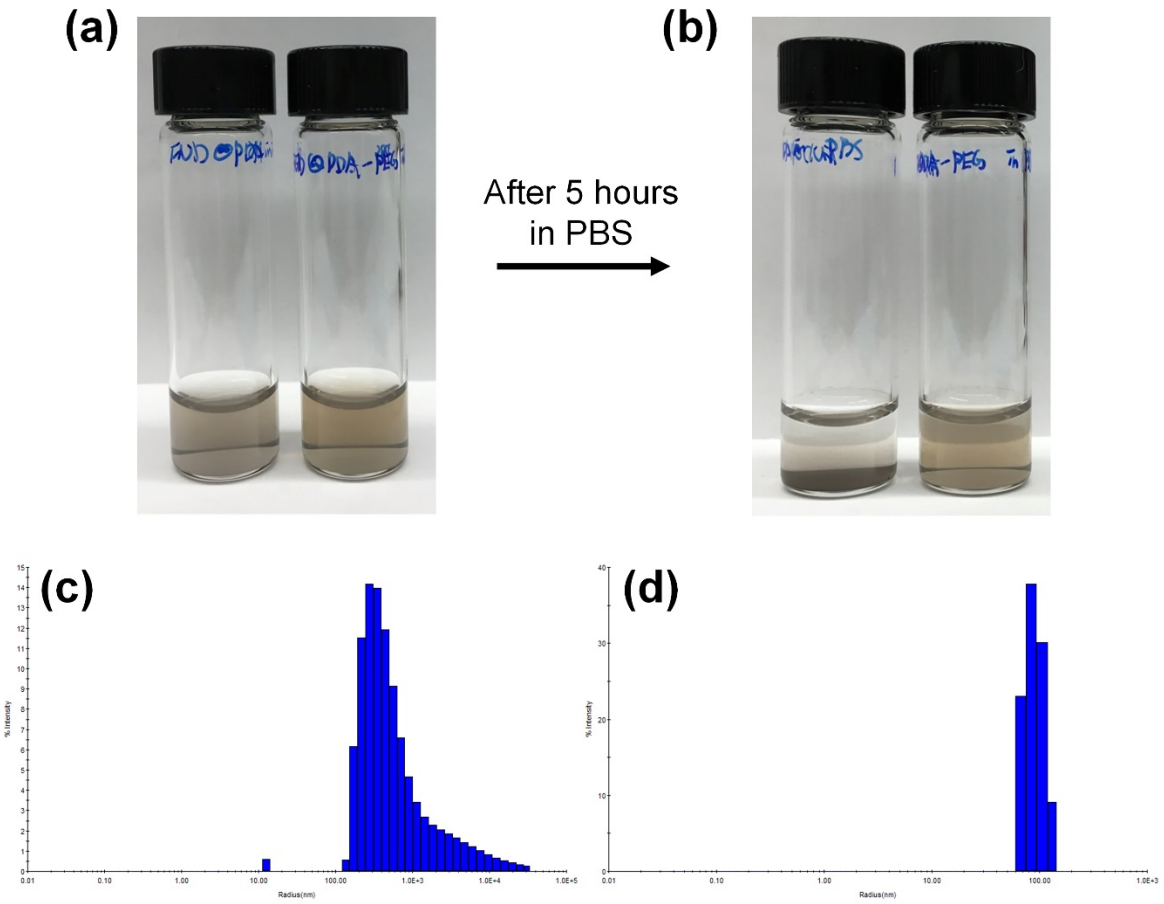

Figure S4. Photographs of FND@PDA and PEGylated FND@PDA (a) as prepared and (b) after 5 hr in PBS. DLS results of (c) FND@PDA and (d) FND@PDA-PEG after 5 hr in PBS.

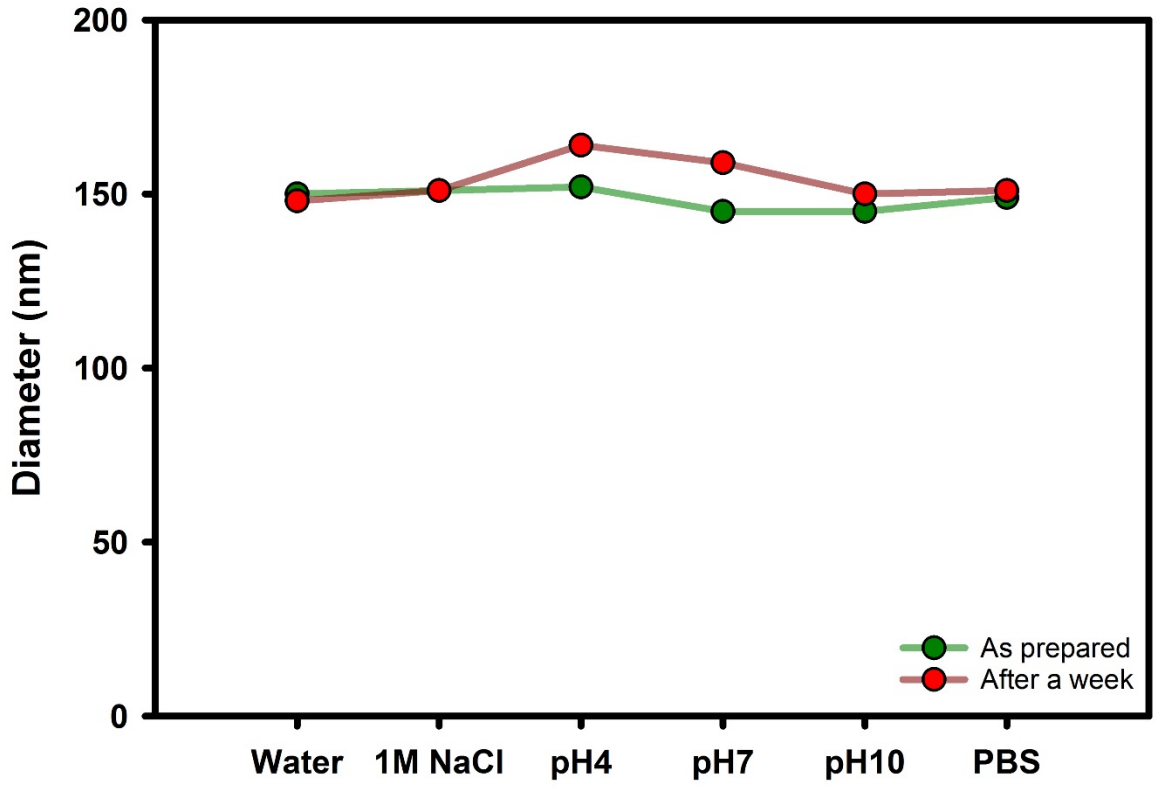

Figure S5. Colloidal stability of PEGylated FND@PDA at pH 4, 7, and 10 (pH adjusted using HCl and NaOH solutions with PBS buffer), in 1M NaCl, PBS buffer. DLS measurements were performed as prepared (green) and after one week in buffer (red) (The PEGylated FND@PDA was stored in PBS buffer for 1 month).

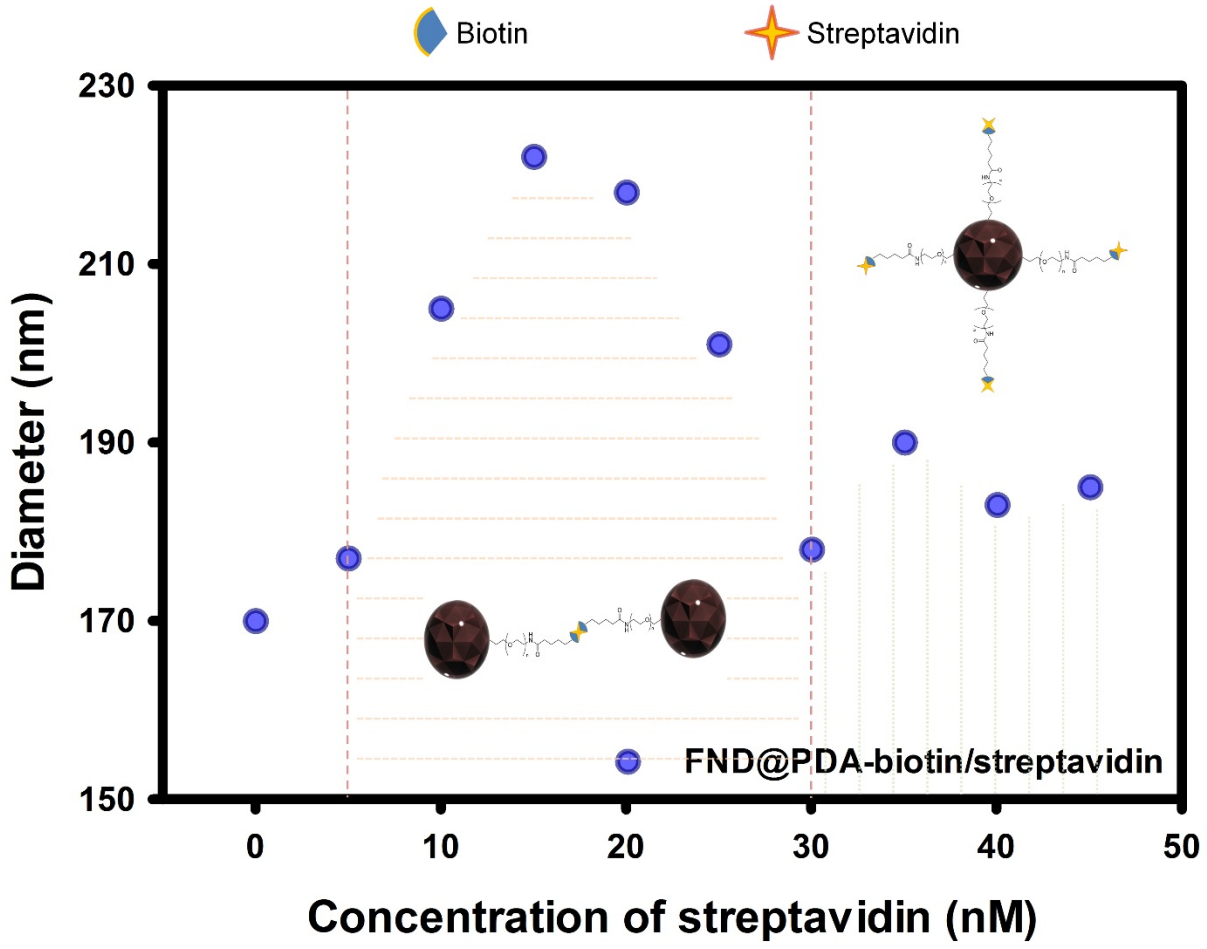

Figure S6. DLS-based determination of biotin on FND@PDA-PEG-biotin. Due to the tetravalency of SA, biotinylated FNDs will aggregate for concentrations of SA that are lower than the biotin surface concentration of the biotin FNDs. Once the surface bound biotins are saturated with SA, the biotin FNDs no longer aggregate. The SA concentration-dependent aggregation and saturation can be followed via DLS measurements of the hydrodynamic diameter of the biotin-FNDs mixed with different concentrations of SA. For individual samples mixed with increasing concentrations of SA, there is an initial increase in diameter corresponding to aggregation (left shaded region) (inset schematic) followed by a decrease in the diameter to a plateau that remains essentially constant, thought slightly larger than the initial diameter, with increasing SA concentration (right shaded region). The SA concentration at which diameter reached the plateau

value corresponds to the saturation point of the surface biotins (right inset schematic). This concentration divided by the concentration of the FNDs, gives the average number of biotins on the FNDs.

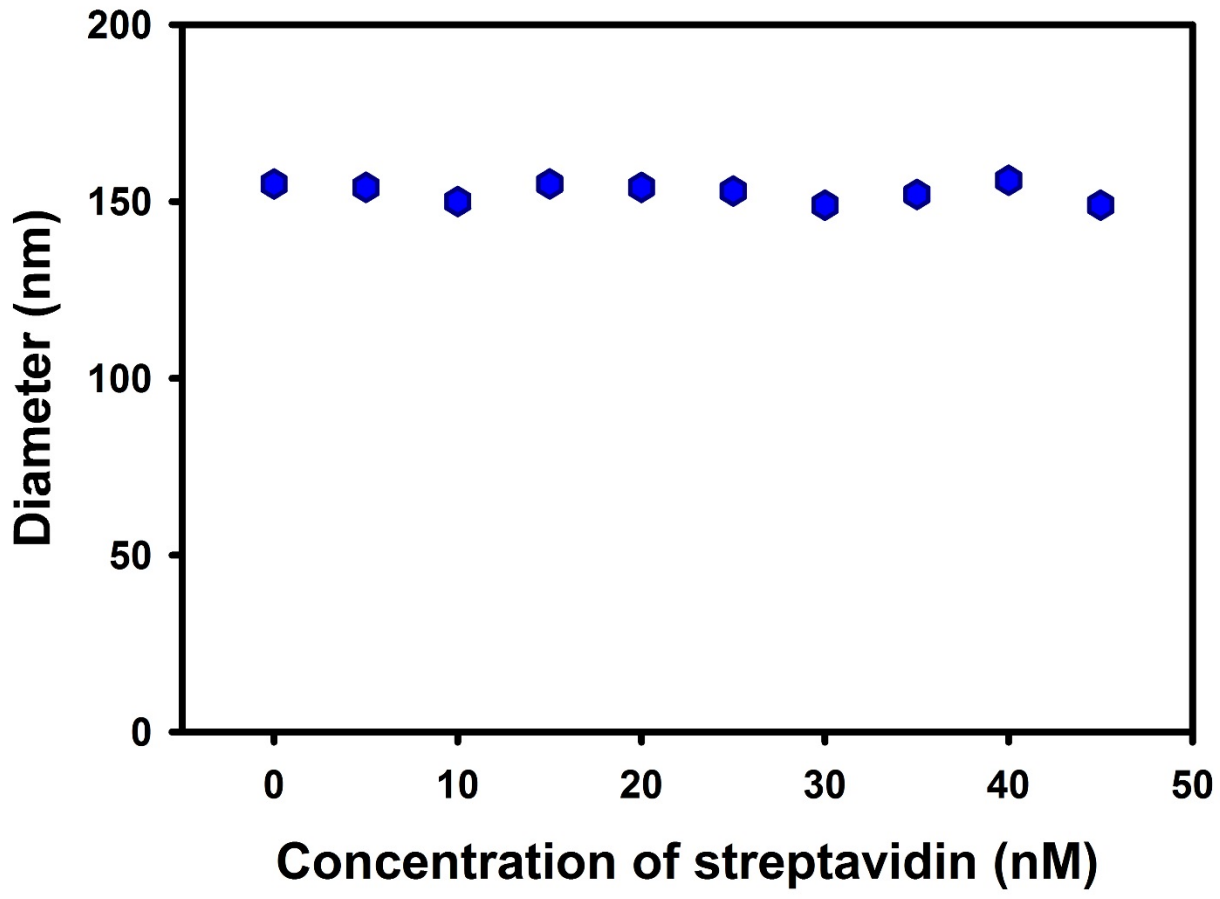

Figure S7. Hydrodynamic radius of SA treated FND@PDA as function of SA concentration.

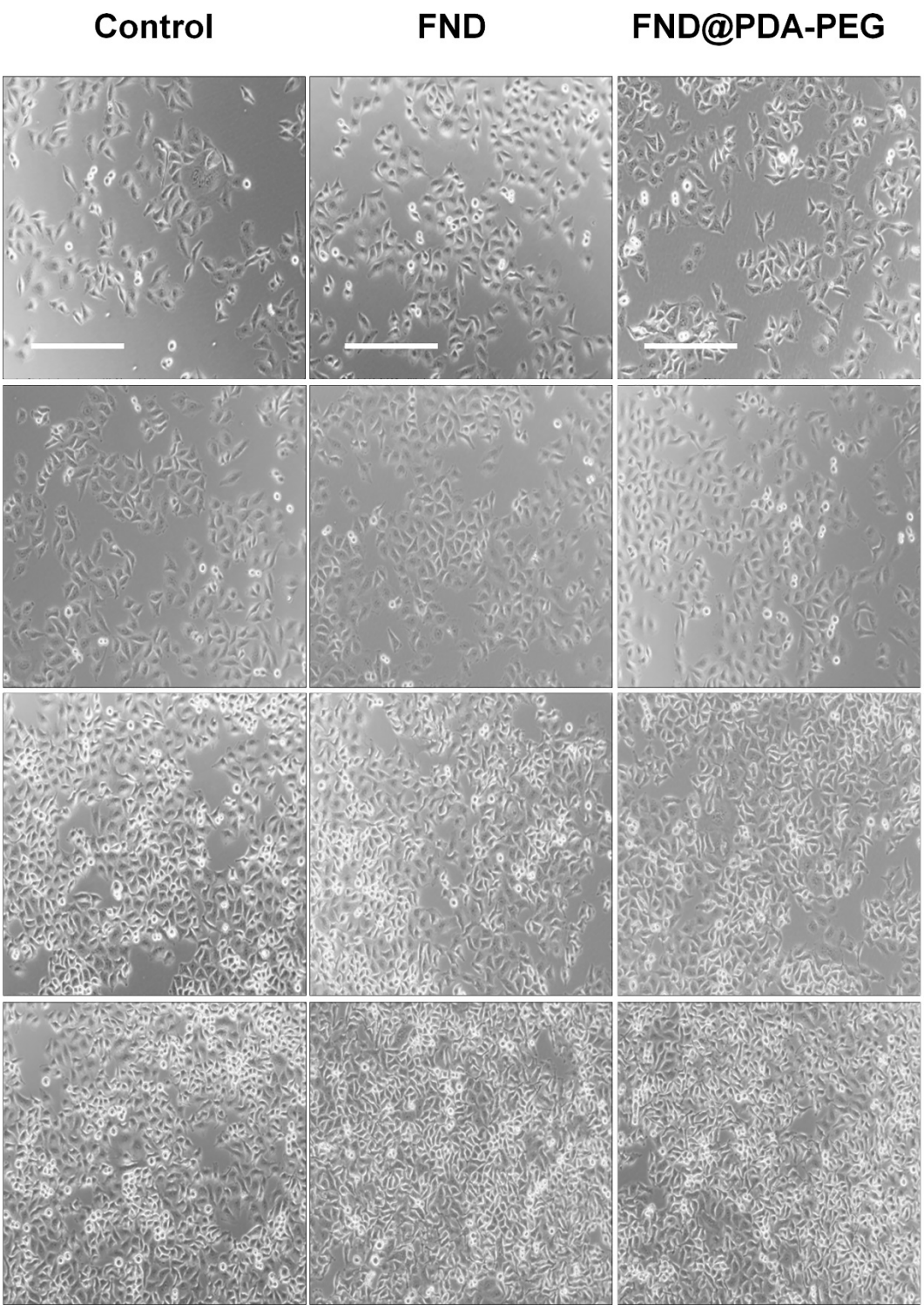

Figure S8. A comparison of the morphology and proliferation of HeLa Cells in the presence of bare FND and PEGylated FND@PDA (50 μg/mL) as function of incubation time (3, 6, 12, and 24 hr after the treatment of nanoparticles). Scale bars represent 500 μm.

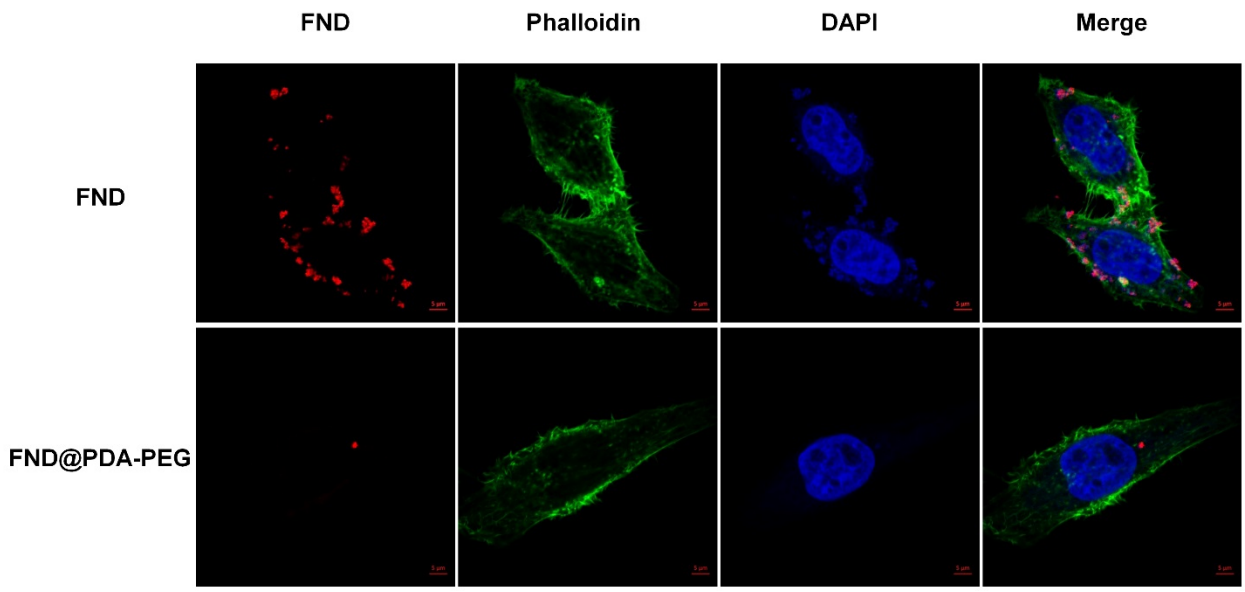

Figure S9. Confocal laser scanning microscopy images of bare FND and PEGylated FND@PDA preincubated in PBS and introduced with HeLa cells. Imaging conditions are described in the methods in the main text and are identical to Fig. 5 in the main text.